



Article

# Sensitivities of Geometric Parameters and Inlet Conditions on the Flow-Heat Characteristics of the Precooler in SABRE

Weiwei Cui 1,\* , Zongming Li 2, Xiaorong Xiang 3,\* , Guoli Pang 2 and Laishun Yang 1

- College of Energy Storage Technology, Shandong University of Science and Technology, Qingdao 266590, China; yangls@sdust.edu.cn
- College of Civil Engineering and Architecture, Shandong University of Science and Technology, Qingdao 266590, China; lzm000206@163.com (Z.L.); 15069986388@163.com (G.P.)
- <sup>3</sup> Institute of Engineering Thermophysics, Chinese Academy of Sciences, Beijing 100190, China
- \* Correspondence: cuiweiwei@sdust.edu.cn (W.C.); xiangxiaorong@iet.cn (X.X.)

Abstract: A physical model for the precooler in a SABRE engine was established, and both the influencing degrees and physical mechanisms of inlet conditions and geometric parameters on the flow-heat transfer characteristics of the precooler unit were explored through parametric analysis and sensitivity analysis, respectively. The results demonstrated that the air massflow rate exerted the greatest influence on the total pressure loss coefficient of the precooler unit due to its significant impact on airflow velocity and thermal loading. The inlet total temperature had a dominant effect on heat transfer rate, owing to its substantial influence on air viscosity and thermal loading. Furthermore, both alone and in combination with air massflow rate, inlet total pressure exhibited a greater impact on total pressure loss of precooler unit compared to inlet total temperature and its coupling effects with air massflow rate. In contrast, both air massflow rate and its coupling effects with inlet total temperature significantly affected the heat transfer rate. On the other hand, tube spacing had the most significant impact on both the total pressure loss coefficient and heat transfer rate due to its substantial influence on air throughflow area and acceleration between microtubes. Moreover, the number of tube rows played a predominant role in determining the heat transfer rate of the precooler unit as it caused significant changes in the contact area between the hot air and the microtubes, as well as airflow velocity. However, only two geometric interaction terms (corresponding to interactions between the number of tube rows and tube spacing, as well as between tube spacing and tube diameter) significantly affected the total pressure loss coefficient, and no interaction term was found to be significant for influencing the heat transfer rate. Eventually, two optimal schemes involving inlet conditions and geometric parameters were established to enhance the flow-heat transfer characteristics of the precooler unit.

**Keywords:** precooler unit; flow-heat transfer characteristic; sensitivity analysis; coupling effect



Citation: Cui, W.; Li, Z.; Xiang, X.; Pang, G.; Yang, L. Sensitivities of Geometric Parameters and Inlet Conditions on the Flow-Heat Characteristics of the Precooler in SABRE. *Energies* **2024**, *17*, 5890. https://doi.org/10.3390/en17235890

Academic Editor: Sergio Nardini

Received: 23 October 2024 Revised: 14 November 2024 Accepted: 18 November 2024 Published: 23 November 2024



Copyright: © 2024 by the authors. Licensee MDPI, Basel, Switzerland. This article is an open access article distributed under the terms and conditions of the Creative Commons Attribution (CC BY) license (https://creativecommons.org/licenses/by/4.0/).

#### 1. Introduction

SABRE is a precooled, combined cycle engine developed by Reaction Engines Limited (REL) [1,2]. When operating under Ma5 flight conditions, the incoming airflow temperature in front of the inlet cone can exceed 1000 °C [3–5]. This elevated temperature inflow may significantly degrade compressor performance, leading to a reduction in engine-specific impulse and thrust [6]. Therefore, it is crucial to precool the high temperature incoming flow before entering the air-breathing engine. SABRE accomplishes this by incorporating a precooler between the supersonic intake and the compressor, and effectively cools down the incoming airflow—with temperatures surpassing 1000 °C—to -140 °C, achieving an impressive heat transfer rate of 400 MW [7]. Due to air's relatively low heat transfer coefficient, a substantial heat exchange area is required to meet high power demands [8]. Consequently, the SABRE engine utilizes lightweight materials for its high-performance microchannel heat exchangers to efficiently precool the flowing air.

Energies **2024**, 17, 5890 2 of 23

The unique spiral structure and compact configuration of the precooler not only enhance heat transfer performance, but also inevitably result in higher total pressure loss. However, very limited research has been conducted on the flow-heat transfer characteristics of misaligned tube bundles in the precooler. Zukauskas [9] discussed the flow and heat transfer of misaligned tube bundles in the precooler, deriving empirical relationships for heat transfer and pressure drop while considering fluid properties' influence. Murray [10] developed the JMHX heat exchanger module, with a microtube diameter of 0.38 mm, to investigate microtube heat transfer characteristics; analyzing classical theory's and formulas' applicability for evaluating the heat transfer coefficient and friction factor in microchannel heat exchangers. Li [11] performed experiments and simulations to conduct an error analysis on classical correlation equations used in heat exchanger design, proposing a new correlation equation for staggered tube bundle precoolers with an error margin less than 5%. Gu [12] investigated the air-side thermal-hydraulic characteristics of bare tube and flat finned tube heat exchangers used for precooling aircraft engines; and found that properly designed flat finned tube heat exchangers outperformed bare tube ones. Kritikos [13] utilized precise geometric modeling of heat exchangers and the porous media method to compare the calculated overall Nusselt number, local Nusselt number, and temperature distributions with existing experimental data. The results indicated that both approaches were suitable for conducting comprehensive investigations into the thermal performance of heat exchangers. Wang [14] investigated the coupling characteristics of flow and heat transfer in the SABRE inlet-precooler system, and the findings suggested that decoupling the designs of the inlet and precooler did not effectively mitigate the trade-off between high Mach number heat transfer performance and low Mach number aerodynamic performance. Ding [15] employed a porous model and a dual-cell heat exchanger model to simulate the pressure drop and heat transfer processes, respectively. The study revealed that flux distribution played a pivotal role in influencing the operation of the heat exchanger; while variations in inlet velocity, total temperature, and total pressure could affect both pressure drop and flow distortion. Xie [16] utilized the surface temperature method and logarithmic mean temperature difference method to evaluate the air-side heat transfer characteristics, while examining the influence of parameters such as inlet pressure, inlet temperature, transverse pitch, coolant velocity, and performance variation on the heat transfer efficiency of tube bundles.

In summary, while the precooler effectively enhances the functionality and operational efficiency of the SABRE engine's compression system, there is currently limited research on the correlation between its three-dimensional geometric structure and flow-thermal characteristics. The sensitive geometric parameters and boundary conditions that impact its overall performance are particularly unclear, as well as their degrees of influence on the comprehensive performance of the precooler. Therefore, a comprehensive precooler unit model was established in this paper to elucidate in detail both the physical mechanisms and extent to which key geometric parameters and inlet conditions affect its flow-heat transfer characteristic, utilizing both the parametric analysis and the response surface model analysis, based on numerous sample schemes and their numerical simulation results. Ultimately, an optimal scheme for the precooler unit was determined and verified, providing theoretical support for optimizing its structure and enhancing the overall performance of the SABRE engine.

# 2. Modeling of the Precooler

The precooler in SABRE was manufactured by REL and comprised 28 heat exchange units, with an outer diameter of 900 mm and an inner diameter of 430 mm [1]. Each spiral precooling unit encircled the central axis and formed a structure with circumferentially symmetrical arrangement (shown in Figure 1). Meanwhile, each heat exchange unit consisted of four staggered microtubes arranged as a row of tube bundles. Each heat exchange microtube had a diameter of 1 mm, with a spacing of 2 mm between adjacent microtubes (measured as the distance between their centers). Due to its outer diameter being ten

Energies **2024**, 17, 5890 3 of 23

times larger than its wall thickness, the microtube can be simplified as a thin-wall cylinder following Den Hartog's guideline [17]. When operating within the engine, the hot air flows radially inward to the precooler while liquid nitrogen serves as the coolant flowing through spiral microtubes to precool the hot air.

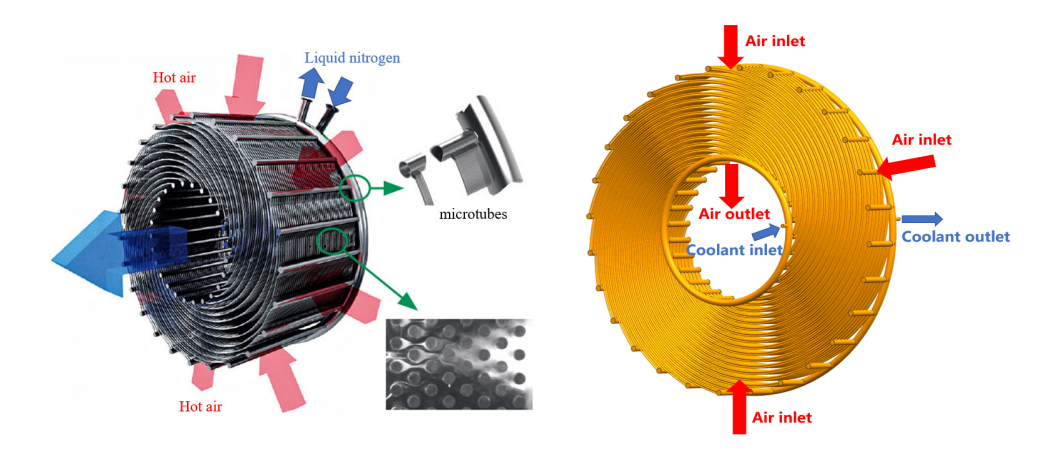


Figure 1. 3D image and physical models of the precooler [1].

Considering the relatively large size of the precooler, which includes numerous cross-flow microtubes, simplification of the computational domain for the precooler structure was necessary. Specifically, due to symmetry along both the axial and circumferential directions, a thin body unit was extracted from its 3-D structure along the axial direction, comprising only two rows of cross-flow microtubes. Subsequently, the thin body unit was divided into 28 symmetrical sector domains along the circumferential direction [18], with one of these domains selected as the final computational domain (shown in Figure 2). Consequently, only ten rows in the radial direction (corresponding to forty staggered microtubes) are included within the sector domain, and the n, d, s in Figure 3 represent the number of tube rows, tube diameter, and tube spacing between adjacent microtubes, respectively. Each of the four staggered microtubes is a row in the sector domain, and the sum of all the tube rows within the sector domain gives the number of tube rows n. The tube spacing s is the linear distance between the centers of adjacent microtubes.

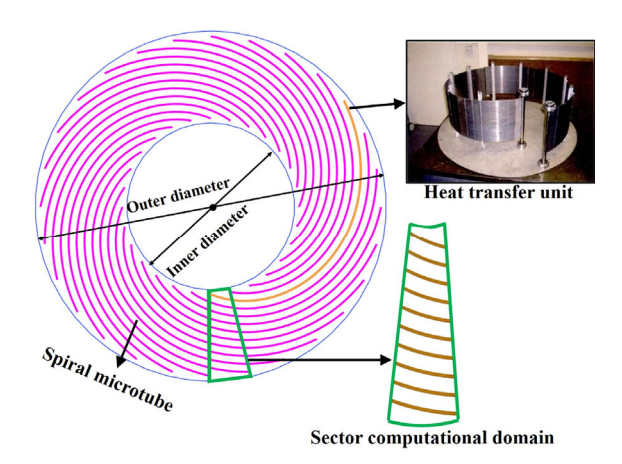


Figure 2. Section view of the precooler and the sector computational domain.

Energies **2024**, 17, 5890 4 of 23

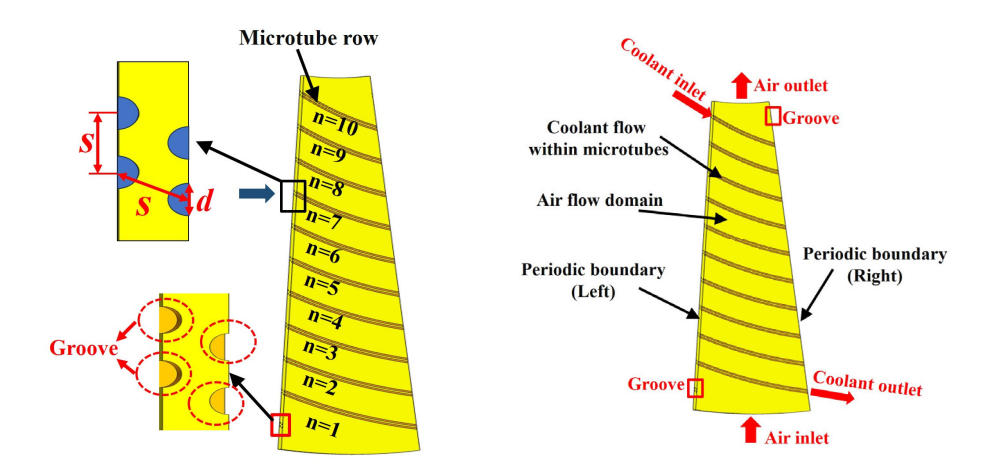


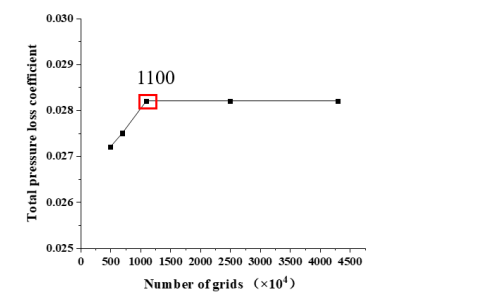
Figure 3. Sector computational domain and the boundary conditions.

A steady-state simulation was conducted in the computational domain of the precooler, solving the Reynolds-averaged Navier-Stokes equations. Specifically, numerical calculations were performed using ANSYS FLUENT 2021 commercial software solver. Liquid nitrogen was utilized as the coolant in the precooler model unit, while air was considered an ideal gas. The inlet of the sector computational domain in the precooler was subjected to boundary conditions, including total temperature, total pressure, and radial flow direction. A boundary condition of massflow rate was imposed on the outlet section. Both the left and right sides were set as periodic boundary conditions, while the two fan-shaped surfaces along the axial direction adopted symmetric boundary conditions. The specific values for inlet total temperature, total pressure, and massflow rate of hot air were determined based on corresponding outlet parameters from a supersonic inlet operating at Ma5 in SABRE engine; and these values were 1181.7 K, 39,993.6 Pa, and 0.0014 kg/s (thin sector body), respectively. Additionally, a geometric structure with a tube spacing of 2 mm, a tube diameter of 1 mm, and 10 tube rows was employed in the prototype scheme of the precooler. Correspondingly, a prescribed massflow rate and a total temperature of 77 K were imposed at the inlet of the microtubes for the coolant (liquid nitrogen), while an outlet boundary condition was set as a pressure of 101,325 Pa. Meanwhile, the flow-thermal characteristics of air and coolant were coupled through heat-loading equilibrium.

The sector computational domain of the precooler unit employed periodic boundary conditions, with a user-defined function (UDF) controlling the temperature at both the inlet and outlet. This ensures that the temperature at each subsequent tube's inlet matches that of its preceding tube's outlet. Figure 3 illustrates the method for establishing these periodic boundary conditions, involving "groove" symmetrically at the first "inlet" and last "outlet" positions of the microtubes. The groove depth is 0.1 mm, which can be disregarded compared to the width of the entire air domain, but allows for periodic symmetry on both sides in this sector computational domain

In order to validate the grid independence, five sets of grids were generated by varying only the overall grid size, while maintaining consistent model, boundary conditions, and turbulence model settings. The numerical simulation results are presented in Figure 4. Upon reaching a grid count of 11 million, further increasing the number of grids had negligible impact on both the total pressure loss coefficient of the precooler unit and heat transfer rate. As a result, a total grid number of 11 million was ultimately selected.

Energies **2024**, 17, 5890 5 of 23



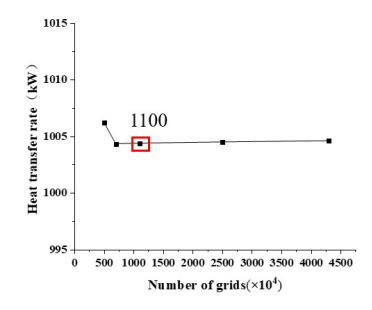


Figure 4. Grid independence verification in sector computational domain.

#### 3. Numerical Method Validation

Since there is no publicly available experimental data on the precooler, a similar model called the experimental module JMHX (described in reference [10]) has been employed for numerical method validation in this study. The JMHX exhibits comparable microchannel layouts and flow characteristics to SABRE's precooler, while also providing geometric and experimental data [10]. Figure 5 illustrates the three-dimensional structure of the JMHX heat exchanger model. The model comprises microtube bundles with a diameter of 0.38 mm, where helium serves as the coolant inside the tubes and nitrogen acts as the hot fluid outside them. Assuming a heat capacity ratio of 1 in numerical simulations, the SST k- $\omega$  turbulence model, incorporating cross-diffusion and propagation of turbulent shear stress [19], demonstrates superior accuracy in fitting the depicted experiment's results, as shown in Figure 6. Consequently, the SST k- $\omega$  turbulence model is adopted in this paper.

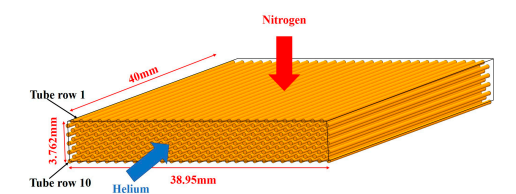
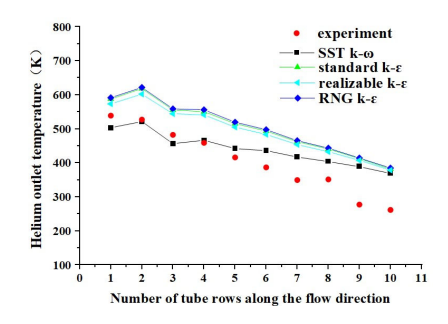


Figure 5. Schematic of the JMHX structure [10].



**Figure 6.** Comparisons of the numerical and experimental results.

## 4. The Influence Rules and Mechanism of Key Factors on Precooler Performance

The flow-heat transfer characteristics of the precooler in the SABRE engine are simultaneously influenced by its primary geometric parameters and inlet conditions. Therefore, a parametric analysis has been employed in this section initially to investigate the influencing mechanism of the variations in the main geometric parameters and inlet conditions on the internal flow-heat transfer characteristics of the precooler.

Energies **2024**, 17, 5890 6 of 23

### 4.1. Effects of Inlet Conditions on the Flow-Heat Transfer Characteristics

The influences of the inlet condition on the flow-heat transfer characteristics of the precooler unit were analyzed by considering three key parameters: air massflow rate, inlet total pressure, and inlet total temperature.

Firstly, three different air massflow rates were imposed on the outlet of the sector computational domain, while keeping the inlet total pressure and temperature constant, to investigate the impact of variations in airflow velocity on the overall performance of the precooler unit. The comparisons of total pressure and temperature distributions within the precooler unit are presented in Figures 7 and 8. As depicted in these figures, an increase in air massflow rate led to a gradual rise in flow velocity, resulting in increased flow resistance and total pressure loss coefficient of the precooler. Consequently, this corresponded to a gradual decrease in total pressure at the outlet of computational domains for all three cases shown in Figure 7. In contrast, the increase in air massflow rate not only significantly contributed to the enhancement of heat transfer rate due to increased airflow velocity (particularly for convective heat transfer coefficient), but also resulted in higher thermal loading carried by hot air. Consequently, the combined effects of increasing air massflow rate led to an elevation in the outlet temperature of the precooler, as shown in Figure 8. Moreover, upon entering the precooler radially (as depicted in Figure 9), the hot air experienced a certain degree of circumferential deflection, leading to slight accumulation of airflow within the right-bottom region of the calculation domain and consequently generating localized high-temperature zones accordingly (indicated by red ellipse in Figure 8).

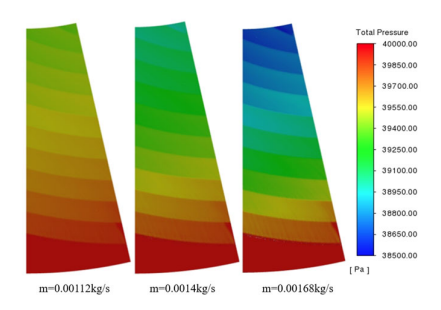


**Figure 7.** Distributions of total pressures in a precooler unit with different air massflow rates.

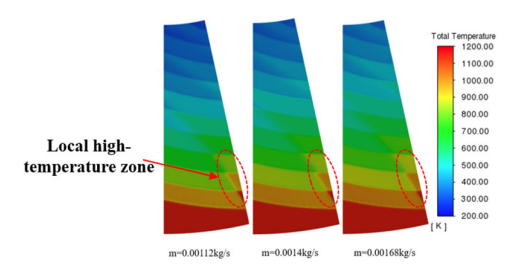


Figure 8. Distributions of total temperature in a precooler unit with different air massflow rates.

Secondly, the inlet total pressure was varied to investigate its impact on the overall performance of the precooler unit, while keeping the inlet total temperature and air massflow rate constant. The distributions of total pressure and total temperature on the cross-section of the precooler unit under different inlet total pressures are illustrated in Figures 10 and 11, respectively. As the inlet air total pressure increased (with relative increments of 20%), there was a corresponding increase in air density, resulting in gradual reductions in both inlet air velocity and flow resistance. Consequently, this led to a decrease in the total pressure loss coefficient of the precooler unit and, ultimately, produced higher outlet values for total pressure (as shown in Figure 10). Conversely, variations in inlet total pressure had only

Energies **2024**, 17, 5890 7 of 23

negligible effects on both the distribution features of total temperature, as well as its outlet values observed from Figure 11.

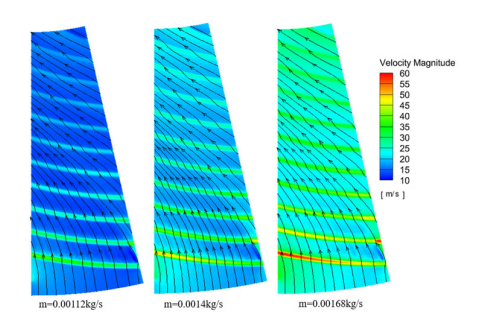


Figure 9. Distributions of spatial streamlines in a precooler unit with different air massflow rates.

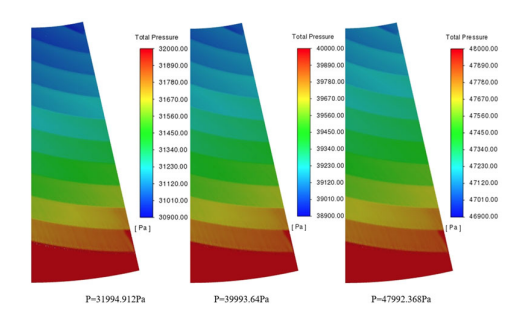


Figure 10. Distributions of total pressures in a precooler unit with different inlet total pressures.

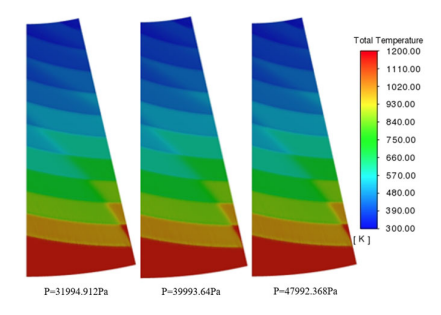


Figure 11. Distributions of total temperatures in a precooler unit with different inlet total pressures.

The distributed contours of total pressures and total temperature on the cross-section of the precooler with different inlet total temperatures are shown in Figures 12 and 13. With the inlet total pressure and air massflow rate remaining unchanged, an increase in the inlet total temperature resulted in corresponding increases in both flow resistance and the total pressure loss coefficient within the precooler. This can be attributed to an accelerated molecular thermal motion at a microscopic level due to higher air inlet temperatures, leading to stronger intermolecular collision effects. Consequently, there was a noticeable increase in air viscosity within the precooler. Additionally, an increase in inlet total temperature caused a decrease in air density, while increasing airflow velocity (with constant air massflow rate and throughflow area). Consequently, the combined effects resulting from the increase in the inlet total temperature led to a further elevation in total pressure loss within the precooler unit. This corresponded to a lower outlet total pressure value for the new case with higher inlet total temperature, as depicted in Figure 12.

Energies **2024**, 17, 5890 8 of 23

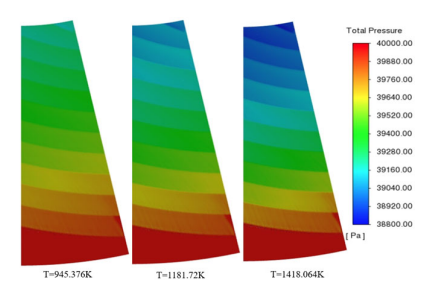
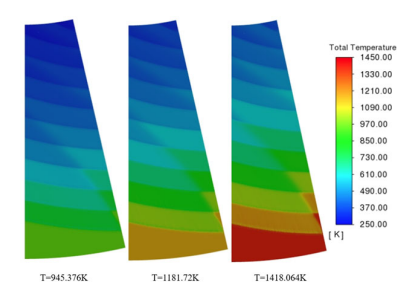


Figure 12. Distributions of total pressures in a precooler with different inlet total temperatures.

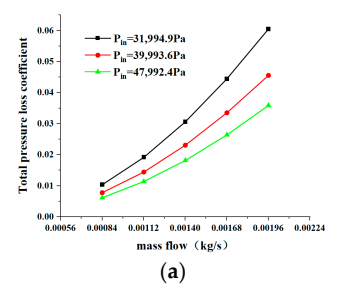


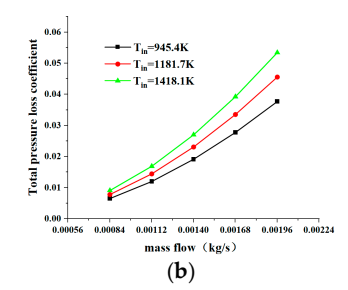
**Figure 13.** Distributions of total temperatures in a precooler with different inlet total temperatures.

Furthermore, it can be observed from Figure 13 that the reduction in airflow velocity caused by increasing inlet total temperature resulted in a higher outlet total air temperature within the computational domain. However, this also led to an increased temperature difference between the inlet and outlet sections of the precooler unit, indicating an augmented thermal loading of incoming hot air due to a larger temperature gradient between the hot air and coolant within the microtubes, and an enhanced heat transfer rate.

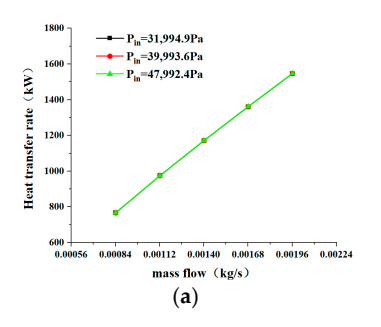
The coupling effects of inlet total pressure, inlet total temperature, and air massflow rate on the total pressure loss coefficient and heat transfer rate of the precooler unit are depicted in Figures 14 and 15. Both the total pressure loss coefficient and the heat transfer rate of the precooler unit exhibited approximately linear increasing trends with an increase in air massflow rate. Moreover, an increase in inlet total pressure attenuated the monotonous rise of the total pressure loss coefficient, while it had no impact on the change in heat transfer rate during an increase in air massflow rate. In contrast, an increase in inlet total temperature contributed to increases in both the total pressure loss coefficient and heat transfer rate of the precooler unit, with a larger increment observed for the latter. Specifically, at any given massflow rate in Figure 15a, a reduction of the inlet total pressure to 31,994.9 Pa resulted in an approximate increase of 32.6% in the total pressure loss coefficient compared to the condition with an inlet total pressure of 39,993.6 Pa; while an increase in the inlet total pressure to 47,992.4 Pa led to a decrease of about 21.2%. Similarly, for a given massflow rate, shown in Figures 14b and 15b, lowering the inlet total temperature to 945.4 K caused a decrease of approximately 17% in the total pressure loss coefficient and a decline of about 22% in heat transfer rate compared to the condition with an inlet total temperature of 1181.7 K. Conversely, raising the inlet total temperature to 1418.1 K resulted in an increase of around 17% in the total pressure loss coefficient and an enhancement of about 22% in the heat transfer rate.

Energies **2024**, 17, 5890 9 of 23





**Figure 14.** Coupling effects of different inlet conditions on total pressure loss. (a) Interactions of total pressure and massflow; (b) Interactions of total temperature and massflow.



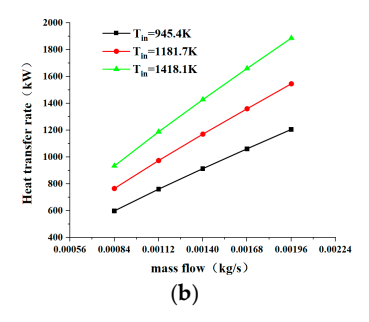


**Figure 15.** Coupling effects of different inlet conditions on heat transfer rate. (a) Interactions of total pressure and massflow; (b) Interactions of total temperature and massflow.

Therefore, it can be inferred that the air massflow rate exerted the greatest influence on both the total pressure loss coefficient and heat transfer rate of the precooler unit. In contrast, the impact of inlet total pressure on the total pressure loss coefficient was more significant than that of inlet total temperature, while it had an almost negligible effect on the heat transfer rate of the precooler unit; which was opposite to the impact of the inlet total temperature on the heat transfer rate. Moreover, it became evident that the interaction effects between inlet total pressure and air massflow rate had a stronger influence on total pressure loss and a weaker influence on the heat transfer rate of the precooler unit compared to interactions between the inlet total temperature and air massflow rate.

#### 4.2. Effects of Main Geometric Factors on the Flow-Heat Transfer Characteristics

By conducting an analysis of the geometric parameters that determined the three-dimensional geometry of the precooler, three primary geometric parameters—tube spacing, tube diameter, and number of tube rows (as shown in Figure 3)—were selected to investigate the impacts of changes in geometric structure on the flow-heat transfer characteristics of the precooler unit.

The distributions of total pressure and total temperature on the cross-section of the precooler unit with different tube spacing are shown in Figures 16 and 17, respectively. It is worth noting that an increase in tube spacing (keeping inlet condition, tube diameter, and number of tube rows constant) inevitably led to an enlargement of the throughflow area perpendicular to the flow direction in the computation domain. This resulted in a reduction in airflow velocity and subsequently decreased the total pressure loss within the precooler, leading to a higher outlet total pressure, as depicted in Figure 16 for cases with larger tube spacing. However, it should be noted that increasing tube spacing also contributed to an elevated outlet total temperature and decreased convective heat transfer coefficient within the precooler unit, as illustrated in Figure 17, due to decreasing airflow velocity.

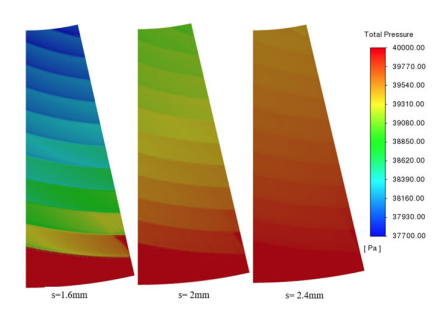


Figure 16. Distributions of total pressures in a precooler unit with different tube spacings.

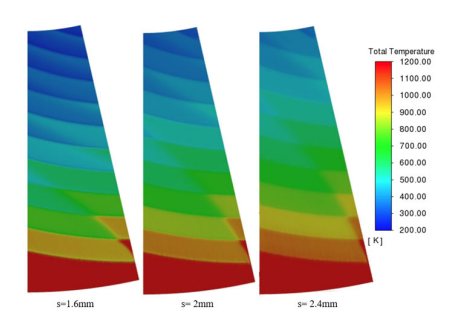


Figure 17. Distributions of total temperatures in a precooler unit with different tube spacings.

The distributions of airflow velocity and spatial streamlines among microtubes within the precooler unit with different tube spacing are shown in Figure 18. As the tube spacing increased from 1.6 mm to 2.4 mm, the flow accelerations between tubes have been weakened significantly, while the wake vortex zone behind each microtube (corresponding to the low-velocity zone) expanded gradually. Consequently, this led to a weakening of the overall heat transfer effect of the precooler. However, although there was an increase in flow losses due to the growing wake vortex zones, these losses were much smaller compared to the total pressure losses caused by airflow interacting with the walls of microtubes. As a result, there was a noticeable reduction in overall total pressure losses occurring due to reduced flow accelerations between tubes.

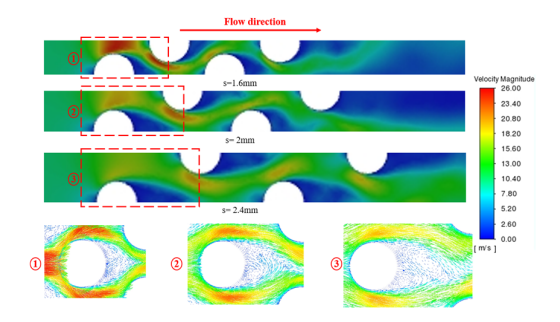


Figure 18. Spatial streamline distributions in a precooler with different tube spacings.

The distributions of total pressure and total temperature on the cross-section of the precooler with different tube diameters are illustrated in Figures 19 and 20, respectively. While keeping the inlet condition, tube spacing, and number of tube rows unchanged, an increase in tube diameter resulted in corresponding rises in both total pressure loss coefficient and outlet total pressure. This phenomenon can be attributed to a reduction in effective throughflow area of hot air relative to an increase in flow velocity between microtubes, leading to significant increases in airflow resistance and convective heat transfer coefficient within the precooler unit. Consequently, smaller outlet total pressure values along with lower outlet total temperatures were observed in all three cases.

Energies **2024**, 17, 5890 11 of 23

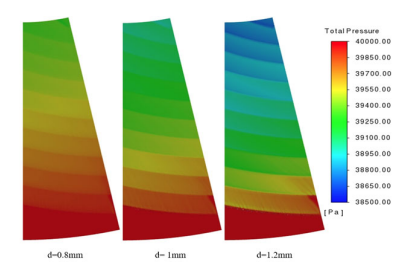


Figure 19. Distributions of total pressures in a precooler unit with different tube diameters.

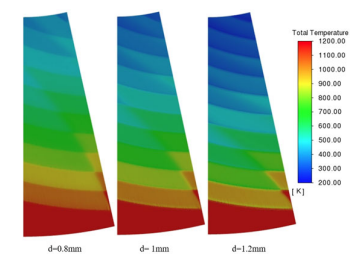


Figure 20. Distributions of total temperatures in a precooler unit with different tube diameters.

In addition to these findings, Figure 21 presents distributions of airflow velocity and spatial streamlines among microtubes within the precooler units with different tube diameters. The results demonstrated that an increase in tube diameter enhanced airflow acceleration within the narrow channels formed by microtubes while reducing wake vortex zones accordingly, which was consistent with the analysis based on Figures 19 and 20.

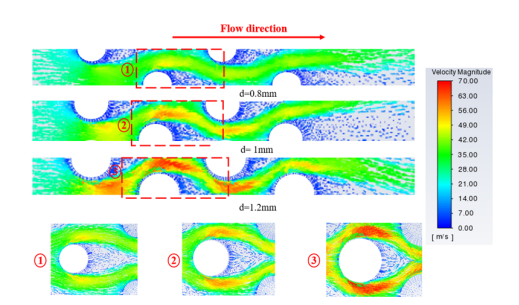
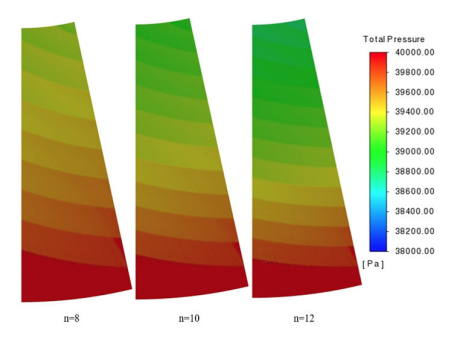


Figure 21. Spatial streamline distributions in a precooler unit with different tube diameters.

The distributions of total pressure and total temperature on the cross-sections of the precooler unit with different numbers of tube rows are illustrated in Figures 22 and 23, respectively (with the inlet conditions, tube spacing, and tube diameter remaining unchanged). Each individual row consists of four microtubes, as depicted in Figures 1 and 2, resulting in numerous acceleration channels between the tubes within each row. Consequently, both the total pressure losses and heat transfer efficiency of inlet hot air gradually increased with an incremental number of tube rows. This led to a smaller outlet total pressure, observed in Figure 22, and a lower outlet total temperature, observed in Figure 23.



**Figure 22.** Distributions of total pressures in a precooler unit with different tube rows.

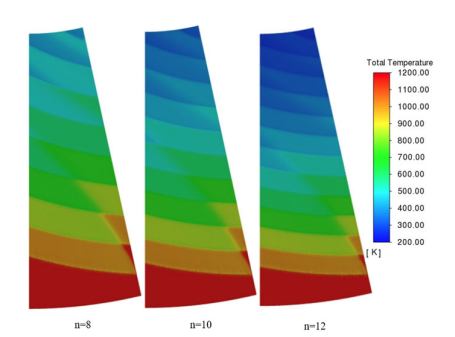
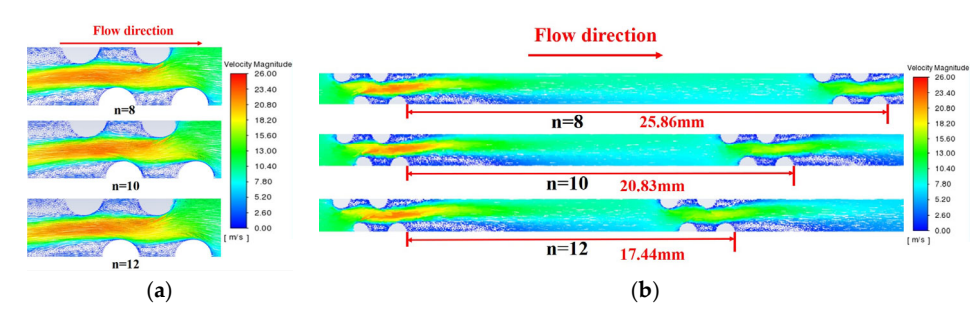


Figure 23. Distributions of total temperature in precooler unit with different tube rows.

The spatial streamline distributions in the precooler unit with varying numbers of tube rows are illustrated in Figure 24. Increasing the number of tube rows alone led to a gradual reduction in the spacing between adjacent tubes among different rows, while keeping both the tube diameter and spacing within each row unchanged; thereby resulting in an augmented total heat transfer area within the precooler unit and consequently improving its heat transfer rate. Since augmenting the number of tube rows did not impact the structural layouts of tube rows within each row, there was minimal disparity observed in flow characteristics among the three cases shown in Figure 24a. Simultaneously, due to relatively large spacing between adjacent tubes from different tube rows, reducing the spacing caused by an increase in tube rows did not affect flow evolution characteristics between adjacent tubes. Therefore, similar flow characteristics were also exhibited across all three cases presented in Figure 24b. However, it is worth noting that increasing the number of tube rows significantly amplified the total heat transfer area within the computational domain, which had a substantial effect on enhancing the heat transfer rate of precoolers.



**Figure 24.** Spatial streamline distributions in a precooler with different numbers of tube rows. (a) Within the tube row. (b) Between the adjacent tubes of different rows.

The coupling effects of tube diameter, number of tube rows, and tube spacing on the flow-heat transfer characteristics of the precooler unit are illustrated in Figures 25 and 26. These figures clearly demonstrated that, in addition to an increase in air massflow rate, enhancing the tube diameter and number of tube rows while reducing the tube spacing

significantly contributed to notable elevations in both total pressure loss coefficient and heat transfer rate within the precooler. Specifically, in comparison to the case with a tube diameter of 1.0 mm, a reduction in tube diameter to 0.8 mm resulted in a decrease of approximately 26.3-28.9% and 6.59-9.71% for the total pressure loss coefficient and heat transfer rate, respectively. Conversely, an increase in tube diameter to 1.2 mm led to an increase of around 29.1–34.8% and 5.1–8.4%, respectively, for these parameters. Similarly, compared to the case with 10 tube rows, reducing the number of rows to 8 caused both the total pressure loss coefficient (by about 22.1–24.1%) and heat transfer rate (by approximately 9.8-12.5%) to decrease; whereas increasing it to 12 resulted in an approximate increase of 19.7–22.8% and 6.8–9.7% for these two parameters. In contrast, when compared to a tube spacing of 2.0 mm, reducing it to 1.6 mm resulted in significant increases in both the total pressure loss coefficient (by 120.3–132.2%) and heat transfer rate (by 4.6–6.0%). Conversely, increasing the tube spacing to 2.4 mm led to notable decreases in these factors by approximately 45.4–47.1% and 5.0–7.6%, respectively. Furthermore, it is worth noting that all changes observed in heat transfer rates were smaller than those seen for total pressure loss coefficients due to the influence of these geometric factors.

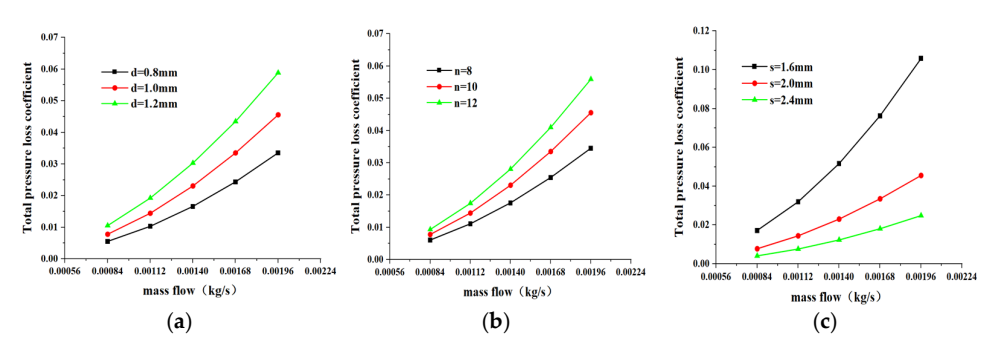


**Figure 25.** Coupling effects of different geometric factors on total pressure loss. (a) Interactions of tube diameter and massflow; (b) Interactions of number of tube rows and massflow; (c) Interactions of tube spacing and massflow.

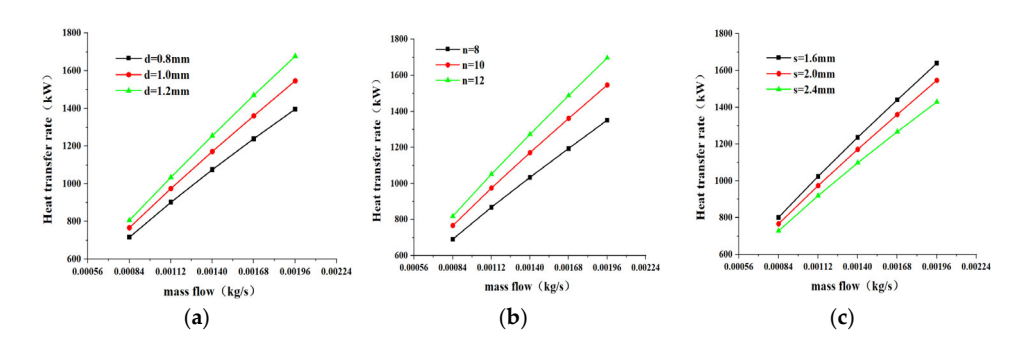


**Figure 26.** Coupling effects of different geometric factors on heat transfer rate. (a) Interactions of tube diameter and massflow; (b) Interactions of number of tube rows and massflow; (c) Interactions of tube spacing and massflow.

Therefore, the preceding analysis has demonstrated significant variations in the degrees of influence exerted by tube diameter, tube row, and tube spacing on the overall performance of the precooler unit. Among these three geometric factors, it is evident that tube spacing exerted the most pronounced impact on the total pressure loss coefficient, followed by tube diameter; whereas the number of tube rows exhibited a comparatively lesser effect. Simultaneously, it can be observed that the number of tube rows predominantly influenced the heat transfer rate of the precooler unit, followed by tube diameter, with relatively minimal impact from tube spacing.

Energies **2024**, 17, 5890 14 of 23

## 5. Identifying the Significant Factors Affecting the Performance of the Precooler Unit

Based on the parametric analysis mentioned above, the Box–Behnken Design (BBD) module of the response surface model (RSM) embedded in Design-Expert 3.0 software was employed to identify the significant factors influencing the flow-heat transfer characteristics of the precooler and further determine their specific degrees of impact.

## 5.1. Sensitivity Analysis of Inlet Conditions

Three experimental variables—namely, inlet total pressure, inlet total temperature, and air massflow rate—were selected to analyze the effects of changes in inlet conditions on internal total pressure loss and heat transfer rate in the precooler unit. These variables were considered as independent factors (A for inlet total pressure, B for inlet total temperature, and C for air massflow rate); each with three levels of sample values. The levels of these factors were adjusted by increasing or decreasing them proportionally by 20% based on the prototype, resulting in a design table consisting of three factors and three levels. The establishment of variable ranges of inlet conditions is based on the actual flight conditions (Ma0 $\sim$ 5) of the SABRE engine and the corresponding outlet parameters of the supersonic inlet upstream of the precooler. Table 1 presents the levels of these factors.

**Factor** Decreasing Prototype Increasing A-inlet total 31,994.9 39,993.6 47,992.4 pressure (Pa) B—inlet total 945.4 1181.7 1418.1 temperature (K) C—air massflow rate 0.00112 0.0014 0.00168 (kg/s)

Table 1. Factors of inlet conditions and three influencing levels.

Two central points were selected and a total of 14 experiment sets were generated. Since these 14 sets mainly focused on the coupling effects among three factors, an additional six sets were established based on these designs, to analyze the influence of single-factor variations on precooler characteristics exclusively. In total, 20 experimental designs were formulated. The details of these experimental designs and corresponding numerical simulation results are presented in Table 2. Herein,  $R_1$  denotes the target of total pressure loss coefficient, while  $R_2$  represents heat transfer rate.

$$R_1 = \frac{P_{in} - P_{out}}{P_{in}} \tag{1}$$

In Equation (1),  $P_{in}$  denotes the inlet total pressure of the precooler unit, while  $P_{out}$  represents the outlet total pressure.

$$R_2 = cM\Delta t \tag{2}$$

In Equation (2), the c, M and  $\triangle t$  represent specific heat capacity of air, air massflow rate, and temperature difference between inlet and outlet sections of computational domain, respectively.

Based on the results in Table 2, an analysis of variance (ANOVA), was conducted to assess the significance of the response surface model and the factors. A higher value for F indicates greater significance for the model under consideration. Furthermore, a p-value was incorporated into ANOVA to estimate the probability of getting the F value of a factor, with the original hypothesis that the factor does not influence the response value, and factors with a p-value less than 0.05 were generally considered as significant items.

The analysis of variance (ANOVA) table for the target of  $R_1$  is presented in Table 3, where a larger F value and smaller p-value indicated greater significance of the related factors. It can be observed from Table 3 that the p-values for inlet total pressure, inlet total

Energies **2024**, 17, 5890 15 of 23

temperature, and air massflow were all less than 0.05, indicating their significant influence. Furthermore, based on the F values, it can be determined that the air massflow rate had the most significant impact on total pressure loss in the precooler; followed by inlet total pressure, and then inlet total temperature. The p-value of the fitted model was less than 0.0001, indicating the high significance of this fitted model.

Table 2. Experimental design schemes and corresponding numerical results.

Scheme	A (Pa)	B (K)	C (×10 <sup>-3</sup> kg/s)	$R_1$	R <sub>2</sub> (kW)
case 1	31,994.9	945.4	1.4	0.025	915.0
case 2	47,992.4	945.4	1.4	0.015	915.0
case 3	31,994.9	1418.1	1.4	0.036	1429.4
case 4	47,992.4	1418.1	1.4	0.021	1429.5
case 5	31,994.9	1181.7	1.12	0.019	974.9
case 6	47,992.4	1181.7	1.12	0.011	975.0
case 7	31,994.9	1181.7	1.68	0.045	1361.8
case 8	47,992.4	1181.7	1.68	0.026	1361.9
case 9	39,993.6	945.4	1.12	0.012	761.6
case 10	39,993.6	1418.1	1.12	0.017	1188.9
case 11	39,993.6	945.4	1.68	0.028	1062.9
case 12	39,993.6	1418.1	1.68	0.039	1661.7
case 13	39,993.6	1181.7	1.4	0.023	1171.8
case 14	39,993.6	1181.7	1.4	0.023	1171.8
case 15	31,994.9	1181.7	1.4	0.031	1171.7
case 16	47,992.4	1181.7	1.4	0.018	1171.8
case 17	39,993.6	945.4	1.4	0.019	915.0
case 18	39,993.6	1418.1	1.4	0.027	1429.4
case 19	39,993.6	1181.7	1.12	0.015	974.9
case 20	39,993.6	1181.7	1.68	0.034	1361.4

Table 3. Variance analysis results of total pressure loss coefficient in precooler unit.

Source	Sum of Squares	Mean Square	F-Value	<i>p</i> -Value
Model	15.7	1.74	1785.5	< 0.0001
A	3.98	3.98	4076.6	< 0.0001
В	1.68	1.68	1718.9	< 0.0001
С	9.50	9.50	9729.8	< 0.0001
AB	0.05	0.05	46.4	< 0.0001
AC	0.27	0.27	271.7	< 0.0001
ВС	0.11	0.11	112.6	< 0.0001
$A^2$	0.08	0.08	83.5	< 0.0001
$B^2$	0.00	0.00	0.03	0.8596
$C^2$	0.04	0.04	40.4	< 0.0001

The coefficient of determination  $R^2$  served as an evaluative metric that reflected the degree to which the regression equation aligned with the data, ranging from 0 to 1. A higher  $R^2$  value indicated a better fitting effect. In this fitted model, the calculated value of  $R^2$  equaling to 0.9994 signified a strong alignment between the predicted and measured values within the experimental range.

Figure 27 illustrates the response surfaces of the total pressure loss coefficient under different inlet conditions. All three interaction items (AB, AC, BC) exerted significant influences on the total pressure loss coefficient. Specifically, decreasing both air massflow rate and inlet total temperature, as well as increasing inlet total pressure, contributed to reducing the total pressure loss coefficient. Table 3 and Figure 27 indicate that the *p*-values of interaction terms AB, AC, and BC were all less than 0.05, indicating their significance on the total pressure loss coefficient. Although considering interactions between two factors resulted in a curved surface shape with certain curvature, all these interaction terms

had reducing significance on overall total pressure loss, compared with the impacts of single-factor effects.

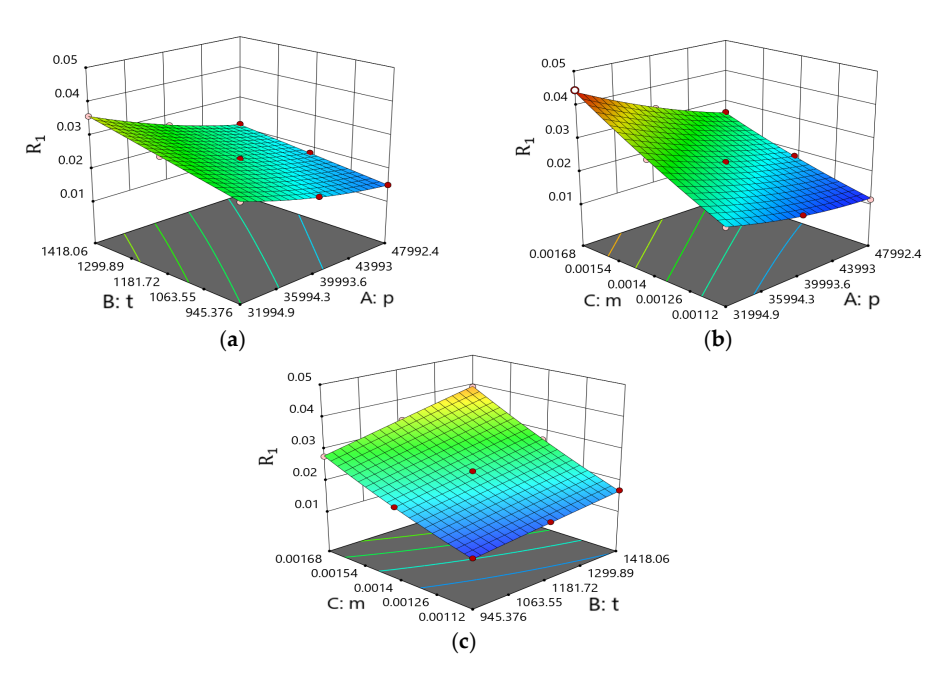


**Figure 27.** Response surfaces of total pressure loss with coupling effects of inlet conditions. (a) Response surface with interactions of inlet total pressure and total temperature. (b) Response surface with interactions of inlet total pressure and air massflow rate. (c) Response surface with interactions of inlet total temperature and air massflow rate.

The analysis of variance table for the  $R_2$  target was presented in Table 4. Both the inlet total temperature and air massflow rate exhibited p-values less than 0.05, indicating their significance as influential factors. Conversely, the p-value for inlet total pressure exceeded 0.05, suggesting it was not the significance for the heat transfer rate of the precooler. Based on the F-values, it can be concluded that inlet temperature had the most substantial influence on the precooler's heat transfer rate, followed by air massflow rate, while the influence of inlet total pressure was not significant. Moreover, this fitted model demonstrated high significance with a p-value less than 0.0001. The  $R^2$  value of this fitted model is 1, demonstrating excellent agreement between the predicted and measured values within the experimental range.

<b>Table 4.</b> Variance analysis of heat transfer rate with different in	nlet conditions.
---	------------------

Source	Sum of Squares	Mean Square	F-Value	<i>p-</i> Value
Model	$1.0 \times 10^{6}$	$1.2 \times 10^{5}$	$8.4 \times 10^{5}$	< 0.0001
A	0.0076	0.0076	0.0557	0.8181
В	$6.6 \times 10^{5}$	$6.6 \times 10^{5}$	$4.8 \times 10^{6}$	< 0.0001
C	$3.7 \times 10^{5}$	$3.7 \times 10^{5}$	$2.7 \times 10^{6}$	< 0.0001
AB	0.0003	0.0003	0.0025	0.9614
AC	0.0015	0.0015	0.0106	0.9201
ВС	7354.46	7354.46	53,592.33	< 0.0001
$A^2$	0.021	0.021	0.15	0.7069
$B^2$	0.9895	0.9895	7.21	0.0229
$C^2$	51.74	51.74	377	< 0.0001

The response surface shapes of heat transfer rate with different inlet conditions are depicted in Figure 28. The *p*-values for the interaction terms of AB and AC, as shown in the figures, were found to be greater than 0.05; indicating their insignificance for the heat

Energies **2024**, 17, 5890 17 of 23

transfer rate. Furthermore, both response surfaces obtained from the interaction terms of AB and AC appeared as planes with minimal curvature, suggesting that these two interaction terms had a negligible impact on the heat transfer rate and were not significant terms. In contrast, it can be observed from Figure 28 and Table 4 that the interaction term of BC exhibited a *p*-value less than 0.05, signifying its significance for the heat transfer rate. Therefore, it appears that the inlet total pressure was not a significant factor either alone or when coupled with other factors, whereas both inlet total temperature and air massflow rate were significant factors, whether acting independently or in combination.

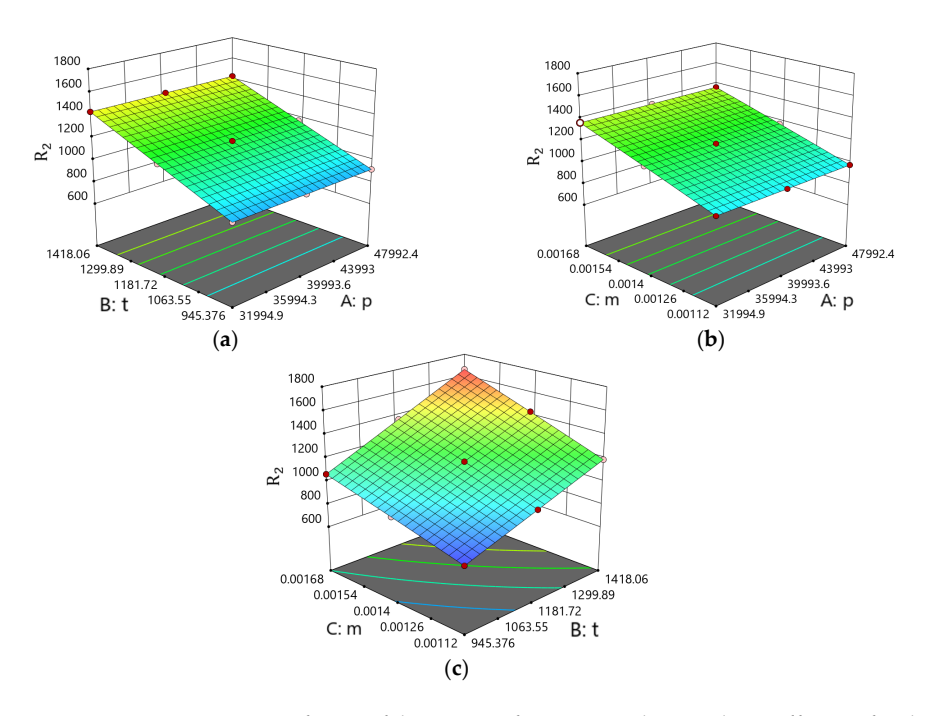


**Figure 28.** Response surfaces of heat transfer rate with coupling effects of inlet conditions. (a) Response surface with interactions of inlet total pressure and total temperature. (b) Response surface with interactions of inlet total pressure and air massflow rate. (c) Response surface with interactions of inlet total temperature and air massflow rate.

According to the sensitivity analysis results recommended by BBD, an optimal combination scheme for the inlet conditions was established. This scheme included an inlet total pressure of 47,992.4 Pa, an inlet total temperature of 1418 K, and an air massflow rate of 0.00112 kg/s. These values corresponded to a predicted total pressure loss coefficient of 0.0132 and a heat transfer rate of 1189.47 kW in the new scheme. Furthermore, numerical simulations were also conducted to determine both the total pressure loss coefficient and heat transfer rate for the optimal precooler unit scheme (as shown in Table 5). The errors between the predicted values and numerical results were found to be within 1%, indicating a high level of accuracy in predictions from analysis of variance.

**Table 5.** Comparisons of predicted and simulated results for optimal scheme of inlet conditions.

	Total Pressure Loss Coefficient	Heat Transfer Rate (kW)
BBD	0.0132	1189.47
CFD	0.0133	1188.96
Errors	-0.68%	0.04%

## 5.2. Sensitivity Analysis of Geometric Factors in Precooler

The number of tube rows (A), tube spacing (B), and tube diameter (C) were designated as three factors with three levels. Each level was adjusted by  $\pm 20\%$  from its original value,

Energies **2024**, 17, 5890 18 of 23

resulting in design schemes with three factors and three levels. The determination of the variable ranges of key geometric factors in the precooler unit is based on the geometric size constraints imposed by the supersonic inlet and its rear transition segment in the SABRE engine. The factor level table is presented in Table 6. The center point number was chosen as two, and an additional six sets of schemes were established to examine the impact of single-factor variations on precooler characteristics. In total, 20 experimental schemes were formed as well. Both the experimental schemes and numerical simulation results are displayed in Table 7. Similarly,  $R_1$  represents the target for total pressure loss coefficient, while  $R_2$  represents the target for heat transfer rate.

**Table 6.** Factors of geometric structure of precooler unit and three influencing levels.

Factor	Decreasing	Prototype	Increasing
A—number of tube rows	8	10	12
B—tube spacing (mm)	1.6	2	2.4
C—tube diameter (mm)	0.8	1	1.2

Table 7. Experimental design schemes of geometric factors and corresponding numerical results.

Scheme	A	B (mm)	C (mm)	$R_1$	R <sub>2</sub> (W)
case 1	8	1.6	1	0.037	1123.4
case 2	12	1.6	1	0.065	1344.6
case 3	8	2.4	1	0.01	964.7
case 4	12	2.4	1	0.015	1201.3
case 5	8	2	0.8	0.013	942.7
case 6	12	2	0.8	0.02	1178.9
case 7	8	2	1.2	0.023	1114.5
case 8	12	2	1.2	0.038	1352.2
case 9	10	1.6	0.8	0.036	1164.5
case 10	10	2.4	0.8	0.009	1000.2
case 11	10	1.6	1.2	0.067	1344.1
case 12	10	2.4	1.2	0.016	1177.4
case 13	10	2	1	0.023	1171.8
case 14	10	2	1	0.023	1171.8
case 15	8	2	1	0.018	1034.9
case 16	12	2	1	0.028	1273.8
case 17	10	1.6	1	0.052	1237.2
case 18	10	2.4	1	0.012	1098.3
case 19	10	2	0.8	0.017	1074.0
case 20	10	2	1.2	0.030	1255.4

The analysis of variance for  $R_1$  due to variations in geometric factors was conducted and presented in Table 8. The p-values associated with the number of tube rows, tube spacing, and tube diameter were all found to be less than 0.05, indicating their significant influences on the total pressure loss coefficient of the precooler unit. Furthermore, based on the p-values obtained, it can be concluded that tube spacing exhibited the most pronounced impact on the total pressure loss coefficient within the precooler unit, followed by tube diameter and then tube rows. Additionally, it is worth noting that this fitted model demonstrated high significance, as indicated by its p-value being less than 0.0001.

Source	Sum of Squares	Mean Square	F-Value	<i>p</i> -Value
Model	54.99	6.11	148.68	< 0.0001
A	4.37	4.37	106.33	< 0.0001
В	37.53	37.53	913.20	< 0.0001
C	6.37	6.37	154.94	< 0.0001
AB	1.35	1.35	32.78	0.0002
AC	0.18	0.18	4.25	0.0662
BC	1.48	1.48	35.93	0.0001
$A^2$	0.004	0.004	0.097	0.7619
$B^2$	3.35	3.35	81.43	< 0.0001
$C^2$	0.004	0.004	0.11	0.7508

**Table 8.** Variance analysis of total pressure loss coefficient with different geometric factors.

The response surface shapes of the total pressure loss coefficient with different geometric factors are illustrated in Figure 29. It can be observed from Table 8 and Figure 29 that the interaction term of AC had an insignificant effect on the total pressure loss coefficient of the precooler unit, as indicated by the nearly flat response surface shown in Figure 29b and the larger *p*-value of more than 0.05. In contrast, both AB and BC interaction terms exhibited *p*-values less than 0.05, indicating their significant impacts on the total pressure loss coefficient. However, despite exhibiting significance in their respective response surfaces formed by these interaction terms (AB and BC), their *F*-values were considerably smaller compared to those of individual factors, suggesting a weakened influence of these two interaction terms on precooler pressure loss.

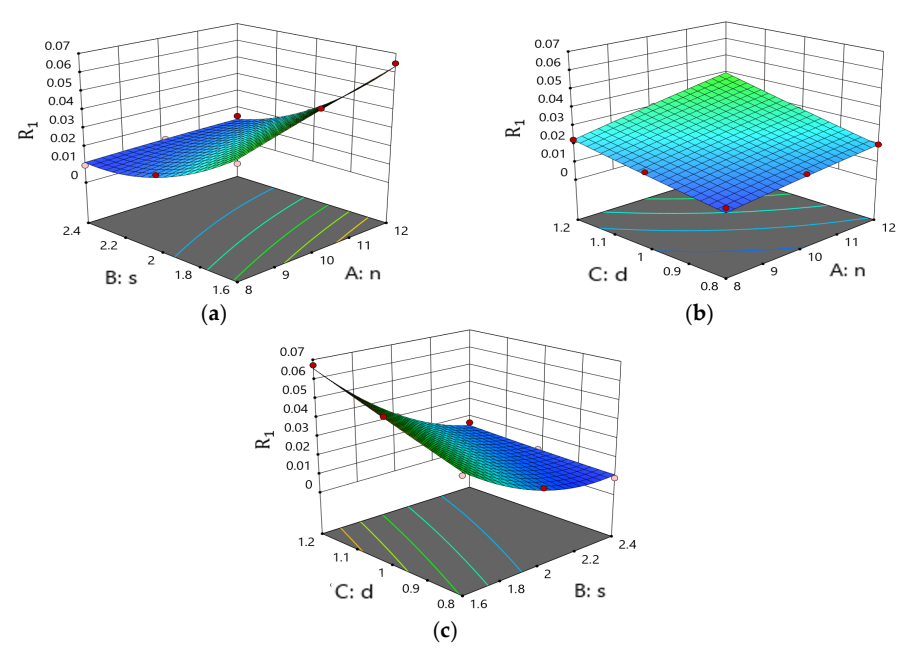


**Figure 29.** Response surfaces of total pressure loss with coupling effects of geometric factors. (a) Response surface with interactions of the number of tube rows and tube spacing. (b) Response surface with interactions of the number of tube rows and tube diameter. (c) Response surface with interactions of tube spacing and tube diameter.

The analysis of variance table for the  $R_2$ , due to variations in geometric factors, is presented in Table 9. The p-values for number of tube rows, tube spacing, and tube diameter were all less than 0.05, indicating their significant influence on the heat transfer rate of the precooler unit. Moreover, based on F-value analysis, it can be concluded that the number of tube rows had a more pronounced impact on heat transfer rate compared to tube diameter, followed by tube spacing. The fitted model's p-value being less than 0.0001 indicated its

Energies **2024**, 17, 5890 20 of 23

significance, and a  $R^2$  value equaling to 0.9984 suggested good fitting between predicted values and actual results within the experimental range.

Source	Sum of Squares	Mean Square	F-Value	<i>p</i> -Value
Model	$2.8 \times 10^{5}$	30,693.3	680.1	< 0.0001
A	$1.14 \times 10^5$	$1.14 \times 10^{5}$	3036	< 0.0001
В	59,581.9	59,581.9	1320.2	< 0.0001
С	78,013.1	78,013.1	1728.6	< 0.0001
AB	59.2	59.2	1.31	0.2788
AC	0.6	0.6	0.013	0.9107
BC	1.4	1.4	0.031	0.8648
$A^2$	1195.8	1195.8	26.5	0.0004
$B^2$	91.3	91.3	2.02	0.1854
$C^2$	76.6	76.6	1.70	0.2218

Table 9. Variance analysis of heat transfer rate with different geometric factors.

Figure 30 illustrates the response surfaces of heat transfer rate with varying geometric factors. As indicated in Table 9, all the *p*-values for the three interaction terms (AB, AC, and BC) were found to be greater than 0.05, suggesting their insignificance in relation to the heat transfer rate. Additionally, the relatively flat shapes in Figure 30 further confirmed that these three interaction terms had minimal impact on the heat transfer rate.

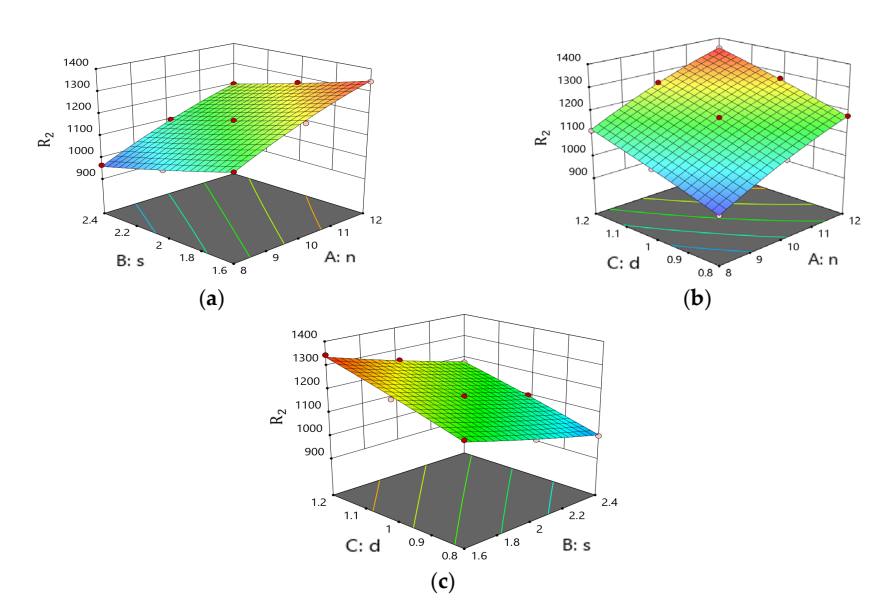


**Figure 30.** Response surfaces of heat transfer rate with coupling effects of geometric factors. (a) Response surface with interactions of the number of tube rows and tube spacing. (b) Response surface with interactions of the number of tube rows and tube diameter. (c) Response surface with interactions of tube spacing and tube diameter.

According to the recommended solution proposed by BBD, an optimal geometric combination scheme was determined, with 12 tube rows, a tube spacing of 2.4 mm, and a tube diameter of 1.2 mm. Consequently, employing this optimal geometric scheme resulted in predicted values for the total pressure loss coefficient and heat transfer rate at 0.0173 and 1285.159 kW, respectively. Furthermore, the numerical simulation was also conducted to validate these predicted solutions, as presented in Table 10; demonstrating that the errors between the predicted results and numerical results for both total pressure loss coefficient and heat transfer rate were within 5%. These findings indicated an acceptable accuracy in predictions derived from analysis of variance.

Energies **2024**, 17, 5890 21 of 23

	Total Pressure Loss Coefficient	Heat Transfer Rate (kW)
BBD	0.0173	1285.16
CFD	0.0181	1279.2
Errors	-4.49%	0.47%

Table 10. Comparisons of predicted and simulated results for the optimal geometric scheme.

#### 6. Conclusions

The degrees of influence and mechanism of inlet conditions and the main geometric factors on the flow-heat transfer characteristics of the SABRE engine's precooler unit were thoroughly elucidated through parametric and sensitivity analyses. Additionally, optimal structural schemes for the precooler were established. The key findings are as follows.

- (1) The air massflow rate exerted the greatest influence on the total pressure loss coefficient of the precooler unit, primarily due to the largest changes in airflow velocity and thermal loading. This was followed by the secondary effect of inlet total pressure, and the tertiary effect of inlet total temperature. In contrast, both the inlet total temperature and the air massflow rate had substantial influences on the heat transfer rate of the precooler unit (with inlet total temperature having a much larger influence than air massflow rate), mainly due to their considerable effects on air viscosity and thermal loading. Conversely, the inlet total pressure had minimal impact on the heat transfer rate.
- (2) The three geometric factors exhibited significant influences on both the total pressure loss coefficient and heat transfer rate of the precooler unit. Furthermore, a ranking was established based on the importance for the total pressure loss coefficient, with tube spacing, tube diameter, and number of tube rows identified as key contributors, due to their impact on air throughflow area and acceleration between microtubes. Similarly, another ranking was determined for the heat transfer rate, highlighting the significance of the number of tube rows, tube diameter, and tube spacing in terms of their influences on the contact area between the hot air and the microtubes, as well as airflow velocity.
- According to the results of the analysis of variance, all pairwise interaction terms among the three factors of inlet conditions were found to be significant for the total pressure loss coefficient of the precooler unit. These interaction terms are ranked in order of significance as follows: interaction term between inlet total pressure and air massflow rate, followed by the interaction term between the inlet total temperature and the air massflow rate, and finally, the interaction term between the inlet total pressure and total temperature rate. However, only the interaction term between the inlet total temperature and the air massflow rate was found to have a significant effect on the heat transfer rate. In contrast, only two interaction terms (corresponding to the interaction term between the number of tube rows and tube spacing, as well as the interaction term between tube spacing and tube diameter) were identified as significant factors affecting the total pressure loss coefficient of the precooler unit. None of these pairwise interactions among geometric factors had a significant impact on heat transfer rate. Furthermore, it is worth noting that all significant interaction terms, regardless of whether they involved inlet conditions or geometric parameters, had much weaker effects on flow-heat transfer characteristics compared to those observed from individual significant factors.
- (4) Two optimal schemes of the precooler unit were eventually proposed, based on sensitivity analysis, to significantly enhance its overall performance. One scheme involved a geometric structure with 12 tube rows, a tube spacing of 2.4 mm, and a tube diameter of 1.2 mm. The other scheme incorporated inlet conditions comprising a total inlet pressure of 47,992.4 Pa, a total inlet temperature of 1418 K, and an air massflow rate of 0.00112 kg/s.

Energies **2024**, 17, 5890 22 of 23

**Author Contributions:** Conceptualization, W.C.; Methodology, Z.L. and X.X.; Software, Z.L.; Validation, G.P.; Investigation, X.X. and G.P.; Writing—original draft, Z.L.; Writing—review & editing, W.C.; Supervision, L.Y.; Funding acquisition, W.C. All authors have read and agreed to the published version of the manuscript.

**Funding:** This research work was sponsored by the National Science and Technology Major Project (Grant No. J2019-II-0014-0035) and the General Program of National Natural Science Foundation of China (Grant No. 52076124).

**Data Availability Statement:** The original contributions presented in the study are included in the article, further inquiries can be directed to the corresponding author.

**Conflicts of Interest:** The authors declare no conflict of interest.

#### Nomenclature

n	Number of microtube rows; number of required experiments
d	Diameters of microtube
S	Tube spacing between adjacent microtubes
$R_1$	Target of total pressure loss coefficient
$R_2$	Target of heat transfer rate
$P_{in}$	Inlet total pressure of the precooler unit
$P_{\text{out}}$	Outlet total pressure of the precooler unit
С	Specific heat capacity of air
$\triangle t$	Temperature difference between inlet and outlet sections of computational domain
M	Air massflow rate
F	Value of the F-test in significance analysis
P	The parameter that determines the result of a hypothesis test
$R^2$	Multiple correlation coefficient
ANOVA	Analysis of variance
RSM	Response surface model/method
BBD	Box-Behnken design module
UDF	User-defined function

## References

- 1. Davies, R.; Bond, A. The SKYLON spaceplane. In Proceedings of the IEE Colloquium on Satellite Launch Vehicles, London, UK, 23 November 1999.
- 2. Varvill, R. Heat exchanger development at Reaction Engines Ltd. Acta Astronaut. 2010, 66, 1468–1474. [CrossRef]
- 3. Zhang, J.Q.; Wang, Z.G.; Li, Q.L. Thermodynamic efficiency analysis and cycle optimization of deeply precooled combined cycle engine in the air-breathing mode. *Acta Astronaut*. **2017**, *138*, 394–406. [CrossRef]
- 4. Luo, J.; Huang, S.; Yang, S.; Zhang, W.; Mu, Z. Effect of Water Injection on Turbine Inlet under Different Flight Conditions. *Energies* **2022**, *15*, 7447. [CrossRef]
- 5. Zeitoun, O. Two-Stage Evaporative Inlet Air Gas Turbine Cooling. Energies 2021, 14, 1382. [CrossRef]
- Dai, J.; Zuo, Q.R. Key technologies for thermodynamic cycle of precooled engines: A review. Acta Astronaut. 2020, 177, 299–312.
  [CrossRef]
- 7. Hempsell, C.M. Progress on SKYLON and SABRE. In Proceedings of the International Astronautical Congress IAC, Beijing, China, 23–27 September 2013; Volume 11, pp. 8427–8440.
- 8. Yu, S.; Jones, T.; Ogawa, H.; Karwa, N. Multi-Objective Design Optimization of Precoolers for Hypersonic Airbreathing Propulsion. *J. Thermophys. Heat Transf.* **2017**, *31*, 421–433. [CrossRef]
- 9. Zukauskas, A.; Ulinskas, R. Heat Transfer in Banks of Tubes in Crossflow; Hemisphere Publishing: New York, NY, USA, 1988.
- 10. Murray, J.J.; Hempsell, C.M.; Bond, A. An Experimental Precooler for Airbreathing Rocket Engines. *J. Br. Interplanet. Soc.* **2001**, *54*, 199–209.
- 11. Li, N.; Zhao, Y.; Wang, H.; Chen, Q.; Li, Z.; Ma, Y.; Tang, G. Thermal and hydraulic performance of a compact precooler with mini-tube bundles for aero-engine. *Appl. Therm. Eng.* **2022**, 200, 117656. [CrossRef]
- 12. Gu, L.D.; Min, J.C. Airside thermal-hydraulic characteristics of compact tube bank heat exchangers used for cooling air from aero engine compressor operating with different compression ratios. In Proceedings of the Asian Conference on Thermal Sciences (1st ACTS), Jeju, Republic of Korea, 26–30 March 2017.
- 13. Kritikos, K.; Albanakis, C.; Missirlis, D.; Vlahostergios, Z.; Goulas, A.; Storm, P. Investigation of the thermal efficiency of a staggered elliptic-tube heat exchanger for aeroengine applications. *Appl. Therm. Eng.* **2010**, *30*, 134–142. [CrossRef]

14. Wang, C.; Eri, Q.; Wang, Y.; Ding, W. Flow and heat transfer characteristics of intake-precooler system for hypersonic precooled aero-engine. *Appl. Therm. Eng.* **2023**, 229, 120596. [CrossRef]

- 15. Ding, W.; Eri, Q.; Kong, B.; Zhang, Z. Numerical investigation of a compact tube heat exchanger for hypersonic pre-cooled aero-engine. *Appl. Therm. Eng.* **2020**, *170*, 114977. [CrossRef]
- 16. Xie, J.; Li, S.; Yan, H.; Xie, G. Numerical analysis on thermal–hydraulic performances of staggered tube bundles for an aero-engine compact precooler. *J. Therm. Anal. Calorim.* **2020**, *141*, 387–399. [CrossRef]
- 17. Den Hartog, J.P. Strength of Materials; Dover Publications: New York, NY, USA, 1961.
- 18. Wang, C.; Eri, Q.; Wang, Y.; Kong, B.; Ding, W. Novel three-dimensional simplified numerical simulation method of a compact precooler for hypersonic precooled air-breathing engine. *Appl. Therm. Eng.* **2023**, 230, 120827. [CrossRef]
- 19. Menter, F.R.; Kuntz, M.; Langtry, R. Ten years of industrial experience with the SST turbulence model. In Proceedings of the 4th of Internal Symposium in Turbulence, Heat and Mass Transfer, Antalya, Turkey, 12–17 October 2003; Volume 4, pp. 625–632.

**Disclaimer/Publisher's Note:** The statements, opinions and data contained in all publications are solely those of the individual author(s) and contributor(s) and not of MDPI and/or the editor(s). MDPI and/or the editor(s) disclaim responsibility for any injury to people or property resulting from any ideas, methods, instructions or products referred to in the content.